





Influence of the Magnetic Sub-Lattices in the Double Perovskite Compound LaCaNiReO₆

Konstantinos Papadopoulos ^{1,*} Ola Kenji Forslund,² Elisabetta Nocerino,² Fredrik O.L. Johansson ^{3,4,5} Gediminas Simutis,^{6,7} Nami Matsubara,² Gerald Morris,⁸ Bassam Hitti,⁸

Donald Arseneau,⁸ Jean-Christophe Orain,⁹ Vladimir Pomjakushin,¹⁰ Peter Svedlindh,¹¹

Daniel Andreica,¹² Lars Börjesson,¹ Jun Sugiyama ¹³ Martin Månsson,² and Yasmine Sassa ^{1,†}

¹*Department of Physics, Chalmers University of Technology, SE-41296 Göteborg, Sweden*

²*Department of Applied Physics, KTH Royal Institute of Technology, SE-106 91 Stockholm, Sweden*

³*Division of Molecular and Condensed Matter Physics, Uppsala University, SE-752 37 Uppsala, Sweden*

⁴*Division of Applied Physical Chemistry, KTH Royal Institute of Technology, SE-100 44 Stockholm, Sweden*

⁵*Sorbonne Universite, UMR CNRS 7588, Institut des Nanosciences de Paris, F-75005 Paris, France*

⁶*Laboratory for Neutron and Muon Instrumentation,*

Paul Scherrer Institut, CH-5232 Villigen PSI, Switzerland

⁷*Department of Physics, Chalmers University of Technology, SE-41296 Goteborg, Sweden*

⁸*TRIUMF, 4004 Wesbrook Mall, Vancouver, BC, V6T 2A3, Canada*

⁹*Laboratory for Muon Spin Spectroscopy, Paul Scherrer Institute, CH-5232 Villigen PSI, Switzerland*

¹⁰*Laboratory for Neutron Scattering and Imaging,*

Paul Scherrer Institute, CH-5232, Villigen, PSI, Switzerland

¹¹*Uppsala University, Department of Engineering Sciences, Uppsala University, 752 36, Uppsala, Sweden*

¹²*Faculty of Physics, Babes-Bolyai University, 400084 Cluj-Napoca, Romania*

¹³*Neutron Science and Technology Center, Comprehensive Research*

Organization for Science and Society (CROSS), Tokai, Ibaraki 319-1106, Japan

(Dated: November 12, 2021)

The magnetism of double perovskites is a complex phenomenon, determined from intra- or inter-atomic magnetic moment interactions, and strongly influenced by geometry. We take advantage of the complementary length and time scales of muon spin rotation, relaxation and resonance (μ^+ SR) microscopic technique and bulk AC/DC magnetic susceptibility measurements to study the magnetic phases of the LaCaNiReO₆ double perovskite. As a result we are able to discern and report a newly found dynamic phase transition and the formation of magnetic domains above and below and above the known ferrimagnetic transition of this compound at $T_c = 103$ K. μ^+ SR, serving as a local probe at crystallographic interstitial sites, reveals a transition from a metastable ferrimagnetic ordering below $T_c = 103$ K to a stable one below $T_{xy} = 30$ K. Furthermore, the fast and slow collective dynamic state of this system is investigated. An evolution of the interaction between Ni and Re magnetic sublattices in this geometrically frustrated fcc structure, is revealed as a function of temperature, through the critical behaviour and thermal evolution of microscopic and macroscopic physical quantities.

I. Introduction

In the research on multifunctional materials, oxides with a double perovskite structure are continuously attracting our interest due to their structural malleability and a multitude of complex physical properties that arise through their magnetically frustrated geometry [1]. Properties such as a magnetoelectric effect, magnetocaloric effect, magnetoresistance or superconductivity may appear in the various phases of perovskite oxides [2–4]. If we are to tune and make use of these properties for real life applications in magnetoelectronics and spintronics, the challenge lies in revealing the static and dynamic processes driven from spin reorientation.

The general composition of this class of materials is $A_2BB'O_6$ where A is an alkaline earth or lanthanide cation, and B, B' are $3d, 4d$ or $5d$ transition metals in various oxidation states, an example of which is illustrated in Figure 1a. The B, B' 1:1 ratio provides an ordering of $BO_6, B'O_6$ edge-sharing octahedra which form two crystallographically distinct sublattices [5]. The structure is flexible to expand, contract or distort from cation displacements, the Jahn-Teller effect or tilting of the octahedra. These distortions are responsible for changes in character of superexchange interactions (ferromagnetic-antiferromagnetic) [6, 7] or the appearance of Dzyaloshinski-Moriya (DM) interactions [8], which significantly alter the physical properties of the perovskite [9]. The magnetic phases of these compounds are controlled both by the magnetic and non-magnetic cations present. More specifically, the sublattice symmetries, the cation's nominal spin and its spin-orbit coupling (SOC) as well as exchange interactions are degrees

*Electronic address: konpap@chalmers.se

†Electronic address: yasmine.sassa@chalmers.se

of freedom that determine the magnetic ground state [10].

In this study we focus on the LaCaNiReO_6 double perovskite and its magnetic behaviour. The crystal structure is that of a rock salt type with two magnetic B, B' cations, in our case Ni and Re respectively as presented in figure 1a. In these transition metal oxide systems, superexchange coupling of neighbouring magnetic ions through shared oxygen typically is the most effective in determining the spin orientation. An interaction between $B-O-B'-O-B$ bonds depends on the bond angle. According to Goodenough-Kanamori (GKA) rules, the interaction is the strongest at 180° and is antiferromagnetic if the virtual electron (e^-) transfer is between overlapping orbitals that are each half filled, but ferromagnetic if the virtual e^- transfer is from a half filled to an empty orbital or from filled to half filled orbital. At 90° the interaction is the weakest and it is favoured to be ferromagnetic [11]. For LaCaNiReO_6 , the bonds are bent to an angle of 152° . Between the half filled e_g orbitals of Ni^{2+} and partially filled t_{2g} orbitals of Re^{5+} , the interaction should favour an antiferromagnetic coupling between nearest neighbours (NN) Ni-Re. In addition there exists a competition between these NN interaction and the longer range, next nearest neighbours (NNN) Ni-Ni and Re-Re. For the 180° NNN bonds, according to GKA, a ferromagnetic coupling is possible.

We suggest a ground state that is determined by two interacting magnetic sublattices where the Ni spins orient antiparallel to the Re spins, while the moments of each individual sublattice order along the same direction. We employed both muon spin rotation/relaxation/resonance (μ^+SR) and magnetometry techniques to identify the types of magnetic ordering. Muons as local probes can extract space and time dependent information of the material's intrinsic magnetic environment in zero applied fields. A muon spin precession frequency is a direct indication of an ordered state, while the signal relaxation provides information of the ordering range and fluctuations [12]. Since the time window of muons is typically $10^{-12} - 10^{-6}s$, these results are correlated to AC and DC magnetization measurements that provide a bulk view of the sample in a $10^{-6}s$ time window, taking into account fast and slow magnetic fluctuations that may occur [12].

This compound shows a ferrimagnetic transition to a long-range, commensurate and dynamically ordered state below $T_c = 103K$. The ferrimagnetic ordering has been proposed in previous studies [6], however, our results suggest that this transition results to a metastable phase. The system is found to undergo a phase transition in its dynamic behaviour between $30 - 70K$. The collective relaxation of the spin lattice towards a thermodynamically stable state is characterized by an intrinsic time constant. This defines the magnetization of the system due to an externally applied magnetic field with specific period and amplitude. Above transition, the (μ^+SR) fits and magnetization measurements support the existence of magnetic domains from $103K$ up to $213K$, while from

$213K$ up to room temperature the paramagnetic phase takes over.

II. Experimental

A polycrystalline sample of LaCaNiReO_6 was prepared in stoichiometric ratio by solid state synthesis. La_2O_3 , SrCO_3 , CaCO_3 , NiO , Re_2O_7 and Re metal were used as the starting materials, forming the final compound through mixing, grinding, pelleting and sintering cycles. X-ray and neutron diffraction patterns were recorded to verify the composition. More information about the synthesis and structure characterization can be found in [6].

Magnetization measurements over a 5-300K temperature range were carried out in a zero-field cooled (ZFC), field-cooled (FCC) or field-warmed (FCW) process. Magnetic field scans were also performed in a $-60-60kOe$ magnetic field range, at various temperatures. The instruments used were a Quantum Design Physical Property Measurement System (PPMS) with a vibration sample magnetometry setup (VSM) as well as a Magnetic Property Measurement Systems (MPMS) Superconducting Quantum Interference Device (SQUID).

The μ^+SR experiments were performed at the surface muon beamline M20 in the TRIUMF facilities. A 100% polarized, continuous, positive muon beam was targeted onto an aluminium coated mylar envelope of approximately $1cm^2$ surface, filled with $\sim 1g$ of the powdered sample. In both instruments the sample was inserted in a 4He cryostat and reached a $2K$ base temperature. The software package *musrfit* was used to analyze the data [13]. Measurements were performed in the zero-field (ZF) and transverse-field (TF), with respect to the initial muon spin polarization. Muons were implanted one at a time into the sample, and come to rest at an interstitial site. There they interact with the local magnetic field, undergoing a Larmor precession and finally emitting a positron, with a high probability in the direction of the spin orientation before decay [12]. Our data sets consists of ~ 10 million positron counts for the TF measurements, and ~ 35 million counts for the ZF measurements.

III. Results

A. Magnetic Susceptibility

Temperature dependent DC magnetic susceptibility was measured from 5-300K with an applied field of 200Oe, as shown in fig.1b. The FCC and FCW curves are identical meaning that there was no quenching of magnetic moments during the cooling. The bifurcation between the FCC and ZFC curves reveals the onset of a magnetic phase at $\sim 213K$. The FC susceptibility at low temperatures reveals a ferromagnetic component and from its first derivative (fig.1b inset) we determine a Curie temperature $T_C = 102.4K$. To extend the results

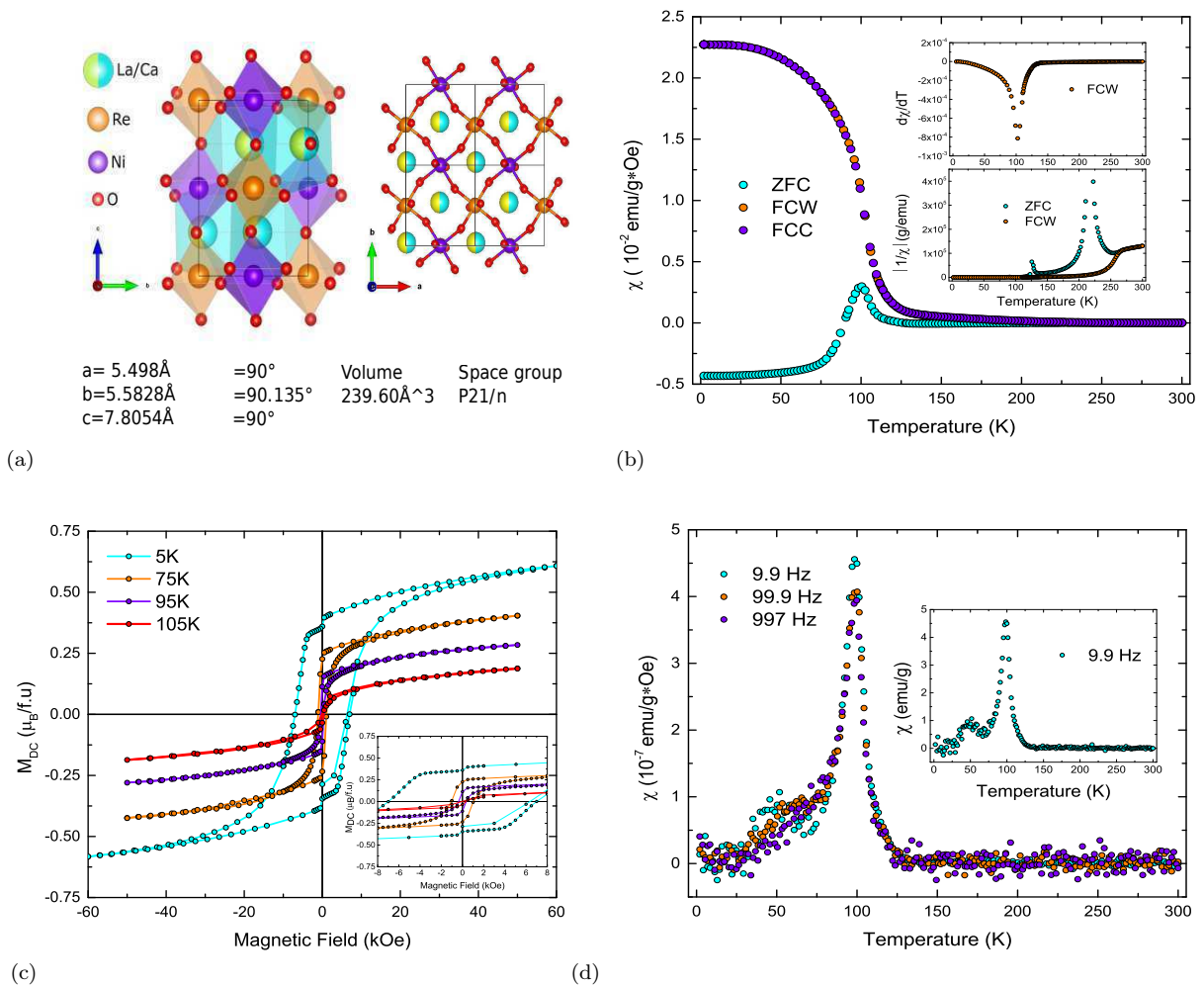


FIG. 1: Crystal structure and magnetic susceptibility of LaCaNiReO_6 . (a) The crystal structure of LaCaNiReO_6 of a geometrically frustrated face-centered cubic crystal lattice with Ni-O and Re-O octahedra. (b) Temperature dependence of the DC magnetic susceptibility in ZFC, FCW and FCC sequences. The insets present the first derivative and the inverse magnetic susceptibility. (c) Magnetic hysteresis loops for 5, 75, 95, 105 K. The inset focuses around the remanence and coercive field regions. (d) AC susceptibility versus temperature for different frequencies. The evolution of susceptibility at 10Hz is also shown independently for clarity.

of the previous study [6] below the Curie temperature, we show explicitly that ZFC susceptibility reaches negative values, in accordance to the net magnetization of the two competing sublattices. This bulk DC magnetic susceptibility sign reversal to negative spontaneous magnetization below T_C can be explained by Neel's molecular field model [14]. A negative exchange coupling between ferromagnetic sublattices or canted antiferromagnetic sublattices are interactions shown to lead to magnetization reversal [15]. In case of N-type ferrimagnetism [16], there exist a compensation temperature T_{comp} , above and below which there is magnetization reversal. In case of a weak and a strong magnetic sublattice, the weak sublattice behaves like a strong sublattice below T_{comp} , while it acts as an exchange-enhanced paramagnetic sublattice

above T_{comp} [17].

The ZFC and FC absolute inverse susceptibility (fig.1b inset) follow the Curie-Weiss law $\frac{1}{\chi} = \frac{T-\theta}{C}$ above 270K. The fit gives a positive Curie-Weiss temperature $\theta = 48.6K$. A positive θ together with a peak in magnetic susceptibility indicate a ferrimagnetic interaction. The calculated effective magnetic moment from this regime is $\mu_{effFCW} = 3.289\mu_B/f.u$ in agreement with the calculated value in [6]. The two peaks at 220K and 125K of the reverse susceptibility curve, correspond to the onset of each one of the two ordered phases.

Isothermal field dependent DC magnetization measurements were performed at 5, 75, 95, 105 and 300K for magnetic fields from -60 to 60 kOe. The evolution of the magnetization is presented in figure 1c (The para-

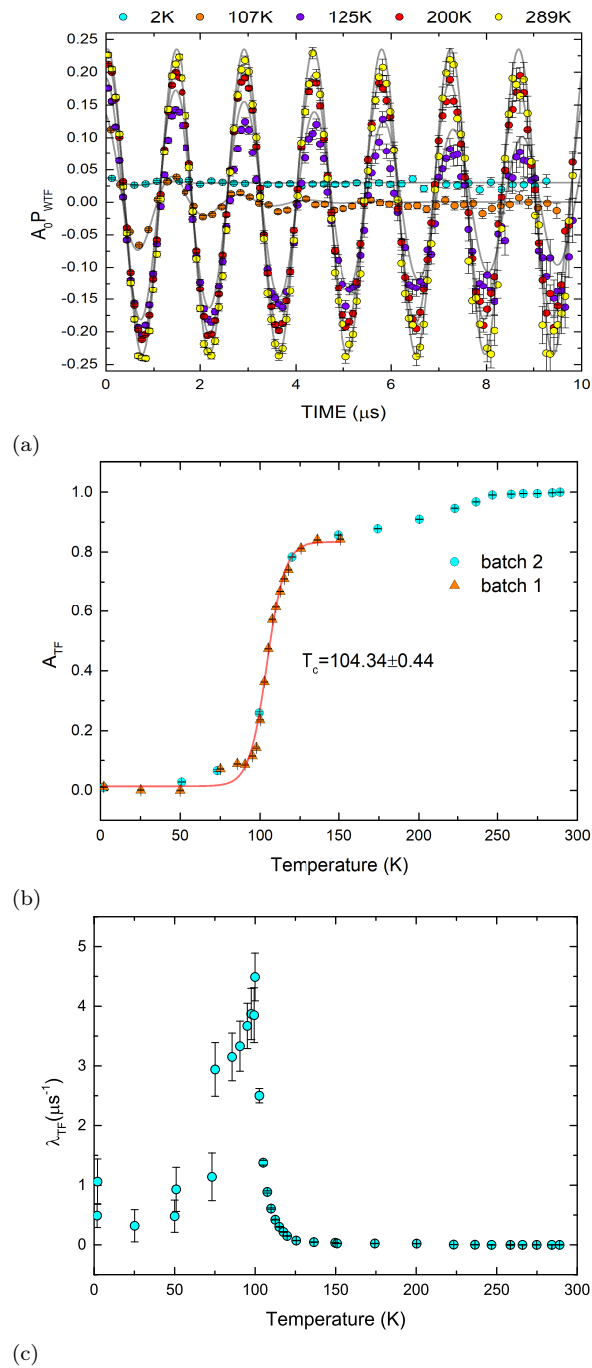


FIG. 2: (a) Weak transverse field (wTF= 50 G) time spectra recorded at $T = 45$ K, 125 K, 200 K and 300 K. The solid lines are fits obtained from Eq. 1. A clear, temperature dependent oscillation is observed. The maximum asymmetry is fully recovered at 290 K. (b) The asymmetry (Eq. 1) versus temperature shows a magnetic transition at 104.34 K with a step at 50 K. A second transition appears also at 230 K. (c) Relaxation of the oscillatory component exhibits a peak around the transition temperature while a shoulder appears near 50 K.

magnetic, linear behaviour at 300K is not shown). Because magnetisation saturation is never reached for ferromagnets, we consider the remanent magnetization and calculate an effective magnetic moment of $\mu_{eff5K} = 0.36\mu_B/f.u$ which is in agreement to results shown in [6]. In the 5K hysteresis loop, shoulders appears at zero field which indicate spin reorientation [18, 19]. In the recorded loops at 75K and above these shoulders disappear while the remanence and coercivity decrease to a soft hysteresis loop at 105K.

AC magnetic susceptibility measurements were also performed at three ac field frequencies, to probe the magnetic relaxation in the two sublattice spin system as shown in figure 1d. We observe for the first time a second peak in the susceptibility curve rises at 50K as the frequency is tuned from 1000Hz to 10Hz. This is possibly an effect of reordering of domain wall spins with a subtle equilibrium, that respond to an ac field. This fluctuation could be another indication of reorientation and freezing of transverse spin components [20].

B. Muon Spin Rotation

The μ^+ SR study consists of weak TF and ZF measurements. We can extract the local field distribution from the time spectra of the decay asymmetry between the surrounding detectors [21]. From the TF spectra we extract the initial and baseline asymmetry which are used as constants when treating the ZF time spectra. The fitted asymmetry for the ensemble in TF maps the magnetic transition through the dephasing of the external signal. The ZF measurement follows in order to gain detailed information about the conditions of magnetic ordering, as well as the intrinsic magnetic fields, arising from nuclear and electronic moments.

1. Weak transverse field (TF)

Muon depolarization spectra were recorded for TF = 50 Oe in the temperature range $45\text{K} \leq T \leq 300\text{K}$. We present the evolution of the TF spectra at selected temperatures, above and below the magnetic phase transition in figure 2a. Following the oscillation that is driven from the applied external magnetic field, the TF time spectra were fitted using an oscillatory component multiplied by a non-oscillatory depolarizing component according to:

$$A_0 P_{TF}(t) = A_{TF} \cos(2\pi ft + \phi) e^{-(\lambda_{TF} t)} + A_{bg} \quad (1)$$

where A_0 is the initial asymmetry and P_{wTF} is the muon spin polarisation function. A_{TF} , f , ϕ and λ_{TF} are the asymmetry, frequency, relative phase and depolarisation rate of the applied TF, while A_{bg} accounts for background. We observe a dumping of the oscillation with decreasing temperature, towards a magnetically ordered state, with an internal field that also takes part, together

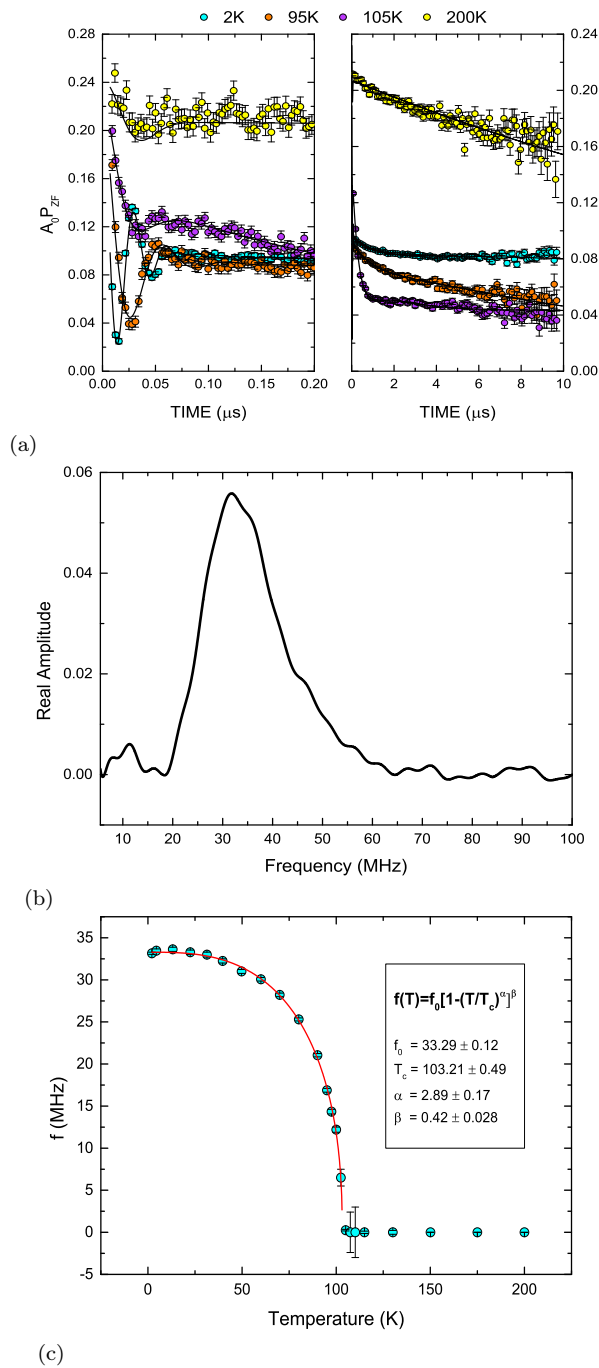


FIG. 3: Zero field time spectra at 2K, 95K, 105K and 200K fitted with Eq. 2. The left and right window present the short and long time domain of the zero field (ZF) time spectrum, respectively. A damped oscillation is observed up to $0.10\mu s$ while the longer time domain displays an exponential relaxation. (b) The real part of the Fourier transform which exhibits the oscillation frequency at 2K. (c) The frequency component is presented as a function of temperature and fitted with the empirical formula 3. A magnetic transition appears at 103.2K where the oscillation of the signal takes effect.

with the applied field. The oscillation frequency is proportional to the applied magnetic field while the asymmetry A_{TF} corresponds to the externally magnetized fraction of the sample. The transverse field asymmetry is displayed as a function of temperature in figure 2b and is fitted with a Boltzmann sigmoid which outputs a transition temperature $T_C = 104.34 K$.

The sample enters the paramagnetic phase and full asymmetry is recovered only above 230 K, a behaviour that corroborates the dc susceptibility measurement. The depolarization rate λ_{TF} is presented in figure 2c. At high temperatures, the damping is approaching zero as the fluctuation of local magnetic moments increases resulting to the motional narrowing effect. As temperature is decreased, λ_{TF} peaks around the magnetic phase transition, at the critical slowing down of magnetic fluctuations. A 50 K shoulder appears, pointing to a dynamic phase transition. Eventually, a commensurate magnetic ordering is achieved at lower temperatures.

2. Zero field (ZF)

ZF measurements were carried out in the temperature range $2 \leq T \leq 200K$. We present a selection of muon spin depolarization spectra at temperatures above and below the magnetic transition in figure 3a. In the short time scale, the onset of a precession and a fast relaxation of the muon spin ensemble can be seen clearly below 105K. This damped oscillation is the effect of a static internal field distribution, perpendicular to the muon spin. In the long time scale, a slower relaxation describes the spin dynamics which corresponds to the longitudinal field components to the muon spin. At base temperature $T = 2K$ an oscillation appears with a single precessing frequency 33.2MHz up to $0.1\mu s$, which denotes a commensurate magnetic ordering.

a. Below the transition temperature.

The time spectrum is fitted with an internal field [22], oscillating function and a Lorentzian Kubo-Toyabe (LKT) function up to 105K:

$$A_0 P_{ZF}(t) = A_{IF} [\xi \cos(2\pi ft + \varphi) e^{-\lambda_T t} + (1 - \xi) e^{-\lambda_L t}] + A_{LKT} \left[\frac{1}{3} + \frac{2}{3} (1 - \Delta t) e^{-(\Delta t)} \right] \quad (2)$$

where A_{IF} is the asymmetry, f the frequency which is a measure of the sub-lattice magnetization, and ϕ the relative phase which is set to zero. The λ_T and λ_L are the transverse and longitudinal depolarization rate applied to the fast precessing part and slow relaxing tail respectively. In the KT function each orthogonal component of the magnetic field at the muon site is represented by a probability distribution with Δ_{KT} , the corresponding distribution width. From DFT calculations on the sister compound $LaSrNiReO_6$ two possible equivalent muon sites were predicted [23]. For the $LaCaNiReO_6$

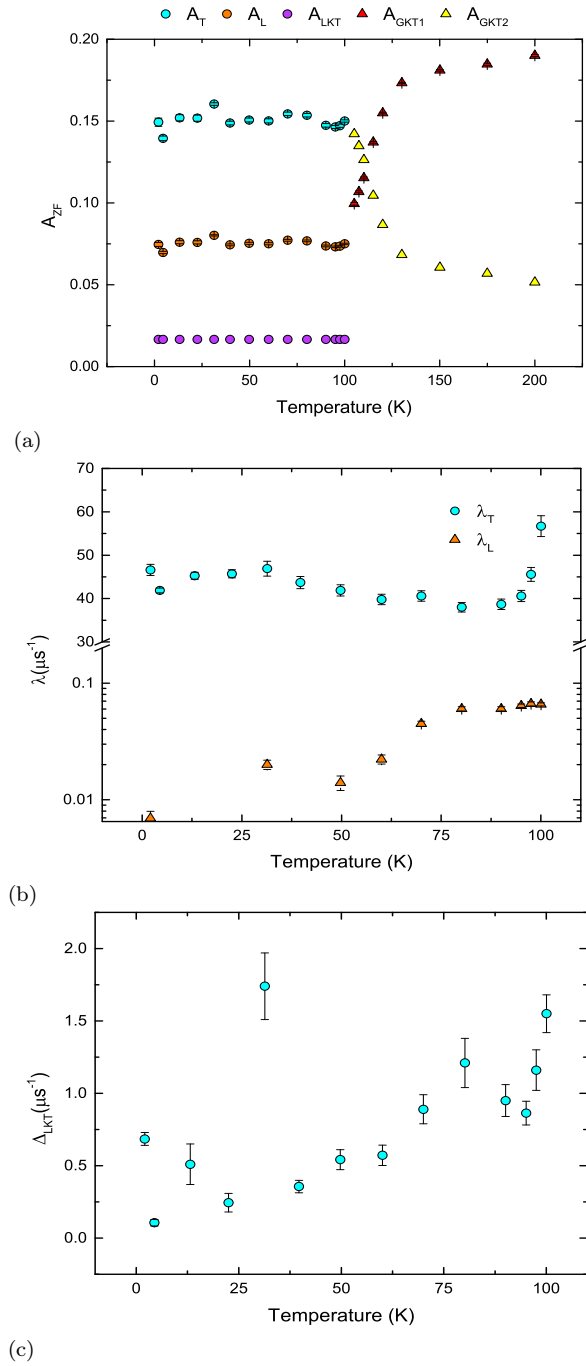


FIG. 4: Fit results for the zero field (ZF) data fitted with Eq. 2. All fit parameters are presented as a function of temperature: (a) Asymmetries for the depolarization contributions to the muon ensembles. (b) The corresponding fast $\lambda_T(T)$ and slow $\lambda_L(T)$ depolarization rates. (c) Field distribution width of the Lorentzian KT fit parameter.

compound one frequency deemed appropriate to reconstruct and translate the data. This precession frequency is clearly indicated in the real part of the Fourier transform, as shown in figure 3b. In figure 3c the frequency extracted from the ZF data, is presented as a function of temperature. The frequency is proportional to the sample magnetization and the experimental data can be fitted by an empirical function that considers both spontaneous magnetization and spin-waves at low temperatures, but also the magnetic anisotropy that becomes significant near the Curie temperature:

$$f(T) = f_0 \left[1 - \left(\frac{T}{T_c} \right)^{\alpha} \right]^{\beta} \quad (3)$$

where $f(0)$ is proportional to the spontaneous magnetization at base temperature and $T_C = 103.21K$ the Curie temperature. This is the actual critical temperature of the sample since the ZF measurement probes the intrinsic magnetic ordering without excitations. The critical exponent α corresponds to the low temperature properties, and β determines the asymptotic behaviour near the transition temperature. The parameter ξ in Eq.2 is used to regulate the $A_T = \frac{2A_{LF}}{3}$ and $A_L = \frac{A_{LF}}{3}$ ratio, describing the perpendicular (precessing) and the parallel (relaxing) tail components. Below transition both A_T, A_L and the contribution from the KT function are constant as illustrated in figure 4a. The A_{LKT} corresponds to a 6% volumic fraction of the sample and the field distribution width narrows down with lower temperatures. This contribution is attributed to randomly oriented dilute spins from a magnetic impurities. Both depolarization rates λ_T, λ_L increase as the temperature approaches the transition, revealing an increase in dynamics. The transverse component has a high value down to base temperature since it depends on the field distribution (fig.4b). The longitudinal component on the other hand slowly approaches zero since the spin dynamics are weaker but still existent(fig.4c).

b. Above the transition temperature.

From 105K to 200K two exponentially relaxing Gaussian Kubo-Toyabe (GKT) are used:

$$A_0 P_{ZF}(t) = A_{KT1} \left[\frac{1}{3} + \frac{2}{3} (1 - \Delta^2 t^2) e^{-\frac{(\Delta t)^2}{2}} \right] e^{-\lambda t} + A_{KT2} \left[\frac{1}{3} + \frac{2}{3} (1 - \Delta^2 t^2) e^{-\frac{(\Delta t)^2}{2}} \right] e^{-\lambda t} \quad (4)$$

Above transition, the signal consists of a rapidly and slowly decaying part as shown in fig.3a, in the long time domain of the zero field time spectra. The fast relaxing part is related to the existence of magnetic domains and fitted with an exponential relaxation function. The relaxation rate decreases fast above transition and the corresponding asymmetry also decreases with higher temperature (fig.5b,4a). The field distribution in this case may be too broad for any oscillatory signal to appear.

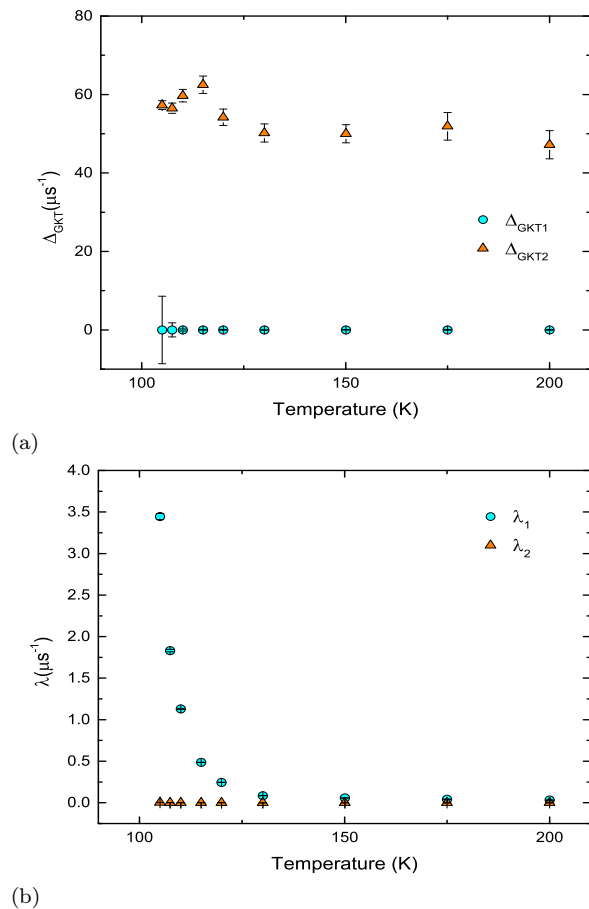


FIG. 5: Temperature dependence of the two relaxing Gaussian KT distributions of Eq. 4. in the temperature range 105 – 200K. (a) The field distribution width of the two KT and (b) the corresponding relaxation rate.

The slowly relaxing part is fitted with a Gaussian Kubo-Toyabe, which describes the paramagnetic contribution to the signal. The width of the field distribution is presented in fig.5a. The corresponding asymmetry increases towards the maximum value at higher temperatures towards 300K where the paramagnetic state is prevalent.

IV. Discussion

Both conventional bulk susceptibility and microscopic muon experiments were used to complete the picture of a long-range ferrimagnetic (FiM) order in LaCaNiReO_6 , established below $T_C = 103\text{K}$. The underlying superexchange interactions between first, second or higher order neighbours define the magnetic ground state. The exchange for a relatively smaller alkaline earth metal results to a different ground state in comparison to its sister compound LaSrNiReO_6 for which an incommensurate magnetic ground state was determined [23]. These

two compounds are a characteristic example proving that superexchange interaction plays a definitive role in magnetic ordering of transition metal oxides.

As GKA rules predict, for a 152° Ni-O-Re angle, there exists an antiferromagnetic (AF) exchange interaction between Ni^{2+} and Re^{5+} [6] ions, a signature of geometrical frustration. The strong spin-orbit coupling of Re atoms, in comparison to Ni ones, reduces the total magnetic moment of the former but also facilitates an anisotropic DM exchange interaction. The long range Ni-Ni and Re-Re interactions in the two sublattices are also significant, as they were described in a similar case for LaSrNiRuO_6 [24]. The NNN couplings are expected to be of ferromagnetic nature, leading to ferromagnetically ordered sublattices that are antiferromagnetically coupled.

In our experiments we followed the evolution of magnetic phases with temperature as each sublattice orders in turn and consequently AF bonds are introduced. Based on the muon signal at ZF, we suggest that magnetic domains exist down to T_c . The depolarization lineshape consists of a highly damped and a slowly relaxing part which correspond to the magnetic domains and the paramagnetic fraction respectively. From the TF measurements (fig.2b) we observe that the full asymmetry is not recovered until above $T = 230\text{K}$ where we enter the paramagnetic state. This evolution is corroborated by the inverse dc susceptibility (fig.1b) behaviour until we reach the region described by the Curie-Weiss law. Below T_c the Ni and Re sublattices order [6, 25, 26] following the mechanism described in N-type ferrimagnetism [16]. This model is also supported by the magnetization reversal in the bulk DC susceptibility results [14].

We now focus on the magnetic ordering below transition. In the recorded hysteresis loop at 5K, shoulders appear at remanent magnetisation. We suggest that the origin of this phenomenon may be an ordering of transverse spin components due to a DM interaction. The monoclinic structure facilitates DM exchange coupling below the ferrimagnetic spin ordering at T_C [27, 28]. The strength of this interaction is proportional to the spin orbit coupling constant which will be significant for the heavy transition metal Re. This interplay may result to a portion of the spin components ordering perpendicular to the pre-existing FiM order at $T_{xy} = 50\text{K}$ (which is further discussed in relation to the $\mu^+\text{SR}$ fit components) as predicted for magnetically frustrated systems [29].

To substantiate this claim we again utilize the ZF μSR technique which is capable to unambiguously separate static from dynamic signatures compared to bulk magnetization measurements. Below T_C an internal field function is sufficiently describing the ZF muon depolarization spectra. An oscillation is clearly observed up to $0.10\mu\text{s}$ at base temperature $T = 2\text{K}$ and the corresponding frequency and asymmetry component display a transition to long range order. This result is in agreement with the DC and AC susceptibility measurements. The dynamic relaxation rates typically peak as the dynamics increase

around transition and decay as the dynamics slow down with decreasing temperature. However both λ_L and λ_T exhibit an increase at $T_{xy} = 50 K$. This may indicate a dynamic phase transition, which can be a signature of transverse spin components that contribute to the static field [29]. A small step at $T = 50 K$ in the frequency as a function of temperature (fig.3c) can also be a signature of this dynamic phase.

In addition, the large deviation between FC and ZFC DC susceptibility below T_C and the appearance of a frequency dependent peak at T_{xy} in the AC susceptibility suggest the presence of magnetic frustration and frozen spin states, which agrees with the appearance of a shoulder in the 5 K hysteresis loop at zero field. This is also pointing to a spin reorientation that can be arguably be linked to the transverse ordering.

V. Conclusions

We have utilised magnetometry and muon spin spectroscopy to elucidate the magnetic properties of the double perovskite compound LaCaNiReO_6 . As the *Ni* and *Re* sublattices successively order, magnetic domains appear as early as at $T = 230 K$ and as the temperature decreases evolves into a long-range commensurate ferrimagnetic order below $T = 103K$. As a result of a partial geometrical frustration of the fcc lattice, we also find combined local and bulk evidence of a dynamic phase of spin clusters for $103K > T > 30K$. A transverse spin freezing at $T_{xy} = 50K$ which does not compromise the long-range ferrimagnetic order down to base temperature

at 2K is a probable scenario. It is surprising that, although both $\text{LaCa}_x\text{Sr}_{1-x}\text{NiReO}_6$, $x = 1, 0$ share a common dilute magnetic phase in the $230K > T > 100K$ region, the substitution of a larger with a smaller diameter alkaline earth drastically facilitates or hinders the formation of long-range order at low temperatures.

Acknowledgments

This research was supported by the European Commission through a Marie Skłodowska-Curie Action and the Swedish Research Council - VR (Dnr. 2014-6426 and 2016-06955) as well as the Carl Tryggers Foundation for Scientific Research (CTS-18:272). J.S. acknowledge support from Japan Society for the Promotion Science (JSPS) KAKENHI Grant No. JP18H01863. Y.S. is funded by the Swedish Research Council (VR) through a Starting Grant (Dnr. 2017-05078) and E.N. the Swedish Foundation for Strategic Research (SSF) within the Swedish national graduate school in neutron scattering (SwedNess). Y.S. and K.P. acknowledge funding a funding from the Area of Advance- Material Sciences from Chalmers University of Technology. D.A. acknowledges partial financial support from the Romanian UEFISCDI Project No. PN-III-P4-ID-PCCF-2016-0112. GS is supported through funding from the European Union's Horizon 2020 research and innovation programme under the Marie Skłodowska-Curie grant agreement No 884104 (PSI-FELLOW-III-3i). All images involving crystal structure were made with the VESTA software [30].

-
- [1] P. M. Woodward, Acta Crystallographica Section B: Structural Science **53**, 32 (1997).
 - [2] D. Marx, P. Radaelli, J. Jorgensen, R. Hitterman, D. Hinks, S. Pei, and B. Dabrowski, Physical Review B **46**, 1144 (1992).
 - [3] K.-I. Kobayashi, T. Kimura, H. Sawada, K. Terakura, and Y. Tokura, Nature **395**, 677 (1998).
 - [4] B. Stojanovic, C. Jovalekic, V. Vukotic, A. Simoes, and J. A. Varela, Ferroelectrics **319**, 65 (2005).
 - [5] M. Singh, K. Truong, S. Jandl, and P. Fournier, Journal of Applied Physics **107**, 09D917 (2010).
 - [6] S. Jana, P. Aich, P. A. Kumar, O. K. Forslund, E. Nocerino, V. Pomjakushin, M. Månsson, Y. Sassa, P. Svedlindh, O. Karis, et al., Scientific reports **9**, 1 (2019).
 - [7] A. A. Aczel, D. Bugaris, L. Li, J.-Q. Yan, C. De la Cruz, H.-C. zur Loye, and S. E. Nagler, Physical Review B **87**, 014435 (2013).
 - [8] W. Zhu, C.-K. Lu, W. Tong, J. Wang, H. Zhou, and S. Zhang, Physical Review B **91**, 144408 (2015).
 - [9] C. Thompson, J. Carlo, R. Flacau, T. Aharen, I. Leahy, J. Pollicemi, T. Munsie, T. Medina, G. Luke, J. Munevar, et al., Journal of Physics: Condensed Matter **26**, 306003 (2014).
 - [10] X. Ding, B. Gao, E. Krenkel, C. Dawson, J. C. Eckert, S.-W. Cheong, and V. Zapf, Physical Review B **99**, 014438 (2019).
 - [11] J. Kanamori, Journal of Physics and Chemistry of Solids **10**, 87 (1959).
 - [12] P. D. d. R. Alain, "muSR:Applications to condensed matter", International series of monographs on physics (Oxford University Press, Oxford, cop. 2011), ISBN 978-0-19-959647-8.
 - [13] A. Suter and B. Wojek, Physics Procedia **30**, 69 (2012).
 - [14] L. Néel, in Annales de Géophysique (1951), vol. 7, p. 90.
 - [15] A. Kumar and S. Yusuf, Physics Reports **556**, 1 (2015).
 - [16] L. Néel, Proceedings of the Physical Society. Section A **65**, 869 (1952).
 - [17] K. P. Belov, Physics-Uspekhi **39**, 623 (1996).
 - [18] M. Ahmed, N. Imam, M. Abdelmaksoud, and Y. Saeid, Journal of Rare Earths **33**, 965 (2015).
 - [19] S. Heisz, G. Hilscher, H. Kirchmayr, H. Harada, and M. Tokunaga, IEEE transactions on magnetics **23**, 3110 (1987).
 - [20] N. Saito, H. Hiroyoshi, K. Fukamichi, and Y. Nakagawa, Journal of Physics F: Metal Physics **16**, 911 (1986).
 - [21] R. L. Garwin, L. M. Lederman, and M. Weinrich, Physical Review **105**, 1415 (1957).

- [22] S. J. Blundell, P. A. Pattenden, F. L. Pratt, R. M. Valladares, T. Sugano, and W. Hayes, *Europhysics Letters (EPL)* **31**, 573 (1995), URL <https://doi.org/10.1209/0295-5075/31/9/012>.
- [23] O. K. Forslund, K. Papadopoulos, E. Nocerino, G. Morris, B. Hitti, D. Arseneau, V. Pomjakushin, N. Matsubara, J.-C. Orain, P. Svedlindh, et al., *Physical Review B* **102**, 144409 (2020).
- [24] X. Ou, F. Fan, X. Chen, T. Li, L. Jiang, A. Stroppa, X. Ouyang, and H. Wu, *EPL (Europhysics Letters)* **123**, 57003 (2018).
- [25] C. Wiebe, J. Greedan, G. Luke, and J. Gardner, *Physical Review B* **65**, 144413 (2002).
- [26] J. Wang, W. Song, and Z. Wu, *physica status solidi (b)* **247**, 194 (2010).
- [27] H. C. Nguyen and J. B. Goodenough, *Physical Review B* **52**, 324 (1995).
- [28] J. B. Goodenough and H. C. Nguyen, *Comptes rendus de l'Académie des sciences. Série II, Mécanique, physique, chimie, astronomie* **319**, 1285 (1994).
- [29] D. Ryan, J. Van Lierop, and J. Cadogan, *Journal of Physics: Condensed Matter* **16**, S4619 (2004).
- [30] K. Momma and F. Izumi, *Journal of Applied Crystallography* **44**, 1272 (2011), URL <https://doi.org/10.1107/S0021889811038970>.